

ARE CLUSTERS STANDARD CANDLES? GALAXY CLUSTER SCALING RELATIONS WITH THE SUNYAEV-ZELDOVICH EFFECT

LICIA VERDE

Princeton University Observatory, Princeton, NJ 08544, USA and
Dept. of Physics and Astronomy, Rutgers University, 136 Frelinghuysen Road, Piscataway NJ 08854-8019

ZOLTÁN HAIMAN¹ AND DAVID N. SPERGEL

Princeton University Observatory, Princeton, NJ 08544, USA
lverde,zoltan,dns@astro.princeton.edu

Draft version October 29, 2018

ABSTRACT

An extensive sample of galaxy clusters will be available in the coming years, detected through their Sunyaev–Zeldovich effect (SZE). We use a semi–analytic model to study the scientific yield of combining SZE data with X–ray and optical follow–up observations. If clusters at a given redshift z_o can be identified with virialized, spherical halos, they populate a well–defined “fundamental plane” (FP) in the parameter space of the three observables: virial temperature (T), total Sunyaev–Zeldovich flux decrement (ΔS_ν), and angular size (θ). The location and orientation of the FP, as well as its redshift–evolution, are sensitive to both the internal evolution of clusters, and to the underlying cosmological parameters. We show that if clusters are not standard candles (e.g. due to feedback, or energy injection), then this can be inferred from the FP. Likewise, we study the dependence of the FP on the cosmological parameters h , σ_8 , and Ω_0 , and quantify constraints on these parameters. We also show that in the absence of any non–gravitational effects, the scatter in the the $(\Delta S_\nu - T)$ plane is significantly smaller than in either the $(\theta - T)$ or the $(\theta - \Delta S_\nu)$ planes. As a result, the $(\Delta S_\nu - T)$ relation can be an exceptionally sensitive probe of both cluster physics and cosmological parameters, and a comparison of the amount of scatter in these three scaling relations will serve as a test of the origin (cosmological vs. stochastic) of the scatter.

Subject headings: Cosmology: theory, cosmological parameters, galaxies: clusters: general

1. INTRODUCTION

Galaxy clusters provide a uniquely useful probe of the fundamental cosmological parameters. The observed abundance of nearby clusters constrains the amplitude σ_8 and slope n of the primordial power spectrum on cluster scales (Evrard 1989, Henry & Arnaud 1991, Bahcall & Cen 1992, White, Efstathiou & Frenk 1993, Eke, Cole & Frenk 1996, Pierpaoli, Scott & White 2000), while the cluster mass function (Lilje 1992, Bahcall & Cen 1993, Viana & Liddle 1996), and its redshift–evolution (Oukbir & Blanchard 1992, Bahcall & Fan 1998, Blanchard & Bartlett 1998, Viana & Liddle 1999, Willick 2000), places useful constraints on the density parameters Ω_0 and Ω_Λ , as well as on the equation of state of the dark energy component (Wang & Steinhardt 1998, Haiman, Mohr & Holder 2001).

The analyses above require an understanding of the internal physics of galaxy clusters, and the extension of the physical properties of the local cluster sample towards higher redshifts. In other words, for cosmological studies, one would ideally like to use clusters as “standard candles”. The central assumptions that make this possible are that clusters are virialized objects at characteristic background densities scaling with redshift as $\rho \propto (1+z)^3$. Under these assumptions, the temperatures, masses and redshifts of clusters are related by the virial theorem. As demonstrated recently by Haiman, Mohr & Holder (2001), the use of large future galaxy cluster surveys for cosmological studies is likely to be limited by the validity of these assumptions, rather than by statistical uncertainties.

Galaxy clusters exhibit various useful scaling relations, such as those between mass and temperature ($M - T$; e.g., Mohr, Mathiesen & Evrard 1999), luminosity and temperature ($L - T$; e.g., Eke, Navarro & Frenk 1998), or size and temperature ($R - T$; e.g., Mohr & Evrard 1997). Analyses of these, and other, similar scalings laws have yielded insight into the physical nature of clusters. In addition, the scaling relations and their scatter also contain useful cosmological information (Verde et al. 2000). The temperature of the hot intra–cluster medium (ICM) is a uniquely direct measure that can be accurately determined from X–ray spectra. On the other hand, the (X–ray) luminosity is sensitive to the density profiles near the cluster core, and the measurements of the masses (from gravitational lensing, or from the velocity dispersion of member galaxies) and radii (e.g., from X–ray isophotes) typically suffer from systematic uncertainties and are thus less robust.

A direct probe of the hot gas in galaxy clusters is provided by the so–called Sunyaev–Zeldovich effect (SZE, Sunyaev & Zeldovich 1980). Cosmic microwave background (CMB) photons interact with the hot ionized intra–cluster gas along their path, distorting the CMB spectrum. In the Rayleigh–Jeans regime, the distortion results in a “decrement” (SZD) of the CMB temperature that depends only on the optical depth to Compton scattering and the cluster temperature, but not on the redshift of the cluster. While the SZE has currently been measured only in a handful of clusters, future SZE surveys can detect rich clusters up to arbitrary redshifts; for example,

¹Hubble Fellow

a recently initiated interferometric survey (Holder et al. 2000), covering 12 deg^2 , will detect hundreds of clusters below redshift $z = 3$.

The SZE can be characterized in two ways: by its "surface brightness" (i.e. the value of the SZ decrement per unit solid angle) near the central region of the cluster, or by its total flux decrement (i.e. the decrement integrated over the whole solid angle of the cluster). While at present SZE studies have mainly used the central SZ decrement, here we propose to use the total SZ flux decrement. This quantity should be a more robust indicator of global cluster properties and has a different dependence on cosmological parameters than the central decrement. However, the total decrement has been difficult to measure to date. Single dish experiments can, in principle, measure the total decrement, but in practice, the need to subtract large backgrounds have resulted in limited signal to noise (Mason et al. 2001; Myers et al. 1997). The most precise SZE observations have so far been obtained with interferometers. Interferometric (Joy et al. 2001; Kneissl et al. 2001; Grego et al. 2000; Reese et al. 2000; Carlstrom et al. 2000; Jones et al. 2001; Birkinshaw 1998 and references therein) observations offer several advantages over observations made with single dishes, in terms of better control over systematics and contamination effects. However, at present, the angular size that can be imaged is small, relative to the angular size of the massive clusters that can be studied at the current sensitivities. Hence, these observations typically do not cover the whole cluster, and instead measure only the central decrement.

The prospects for measuring the total SZ flux decrement will dramatically improve in the next few years. Forthcoming SZE (e.g., DASI, CBI) and cosmic microwave background (CMB) experiments will not only measure the total SZD of an extended cluster sample, but, in many cases, will also resolve the temperature fluctuation over the angular size of the whole cluster.

For example MAP (Bennett et al. 1995) will detect tens of clusters and resolve a few of them; Planck (Bersanelli et al. 1996; Mandolesi et al. 1998) will detect $\sim 10^4$ clusters and resolve and measure the total SZD of 1% of them (Kay, Liddle & Thomas 2001). An experiment such as the proposed Center for study of Cosmic structure (CSCS; Page et al. 2001) could map the CMB anisotropy over 100deg^2 with a resolution of $1.7'$. This would allow *all* galaxy clusters of masses above $4 \times 10^{14} M_\odot$ in the CMB map region to be detected through the SZ effect. The experiment would also determine spectroscopic redshift of more than 300 clusters, and implement X-ray follow up to determine their X-ray temperatures.

In this paper, we investigate the scientific potential of measuring the cluster total SZ flux decrement in the context of a well studied cluster sample for which X-ray and optical follow-up are available. As illustrated in § 3, the total SZ flux decrement (ΔS_ν) is an integrated quantity over the whole cluster, not just along the central line of sight, and should thus be more sensitive to global cluster properties. In particular, ΔS_ν probes a unique combination of the physical parameters of the hot intra-cluster gas, different from those inferred from X-ray observations, and from other data. This allows the construction of new scaling relations. In this paper, we examine these scaling

relations in detail. We are motivated by the forthcoming sample of clusters with measured SZ decrements, as well as by the strong need for observational tests of the assumption that clusters can be used as "standard candles". Our goals are (1) to predict scaling relations that involve the SZD, together with their scatter, and (2) to study how these scaling relations depend on assumptions about the cluster structure (i.e. that clusters are standard candles), as well as on the underlying cosmological parameters. In particular, we quantify these dependencies in the context of a well studied cluster sample, such as those expected to be available in the near future, for which it will be possible to combine SZE and X-ray observations.

This paper is organized as follows. In § 2, we describe our cluster model and its input model parameters. In § 3, we summarize the main observables that the model predicts: redshift (z), virial temperature (T), Sunyaev-Zeldovich decrement (ΔS_ν), and angular size (θ). In § 4, we show that in this model at a fixed z in $(T, \Delta S_\nu, \theta)$ space, clusters are expected to be distributed on a "fundamental plane" with nearly negligible scatter in the $\Delta S_\nu - T$ projection, and that the plane's orientation depends on redshift and on the background cosmology. In § 5, we parameterize deviations from our cluster model caused by additional energy input, or by a lack of full virialization, and quantify their effects on the scaling relations. Similarly, in § 6, we quantify the effects on the scaling relations caused by varying several cosmological parameters. In § 8, we discuss our results and the implications of this work. Finally, in § 9, we summarize our conclusions.

2. MODEL INGREDIENTS

2.1. Spherical Collapse

Generally, galaxy clusters models are based on the collapse of a spherical top-hat perturbation (e.g., Peebles 1980). In this model, the average density $\bar{\rho}_{\text{vir}}$ enclosed within the radius R_{vir} of a cluster of total (dark matter + baryon) mass M_{vir} that forms at redshift z_f is given by (e.g., Kitayama & Suto (1996) hereafter KS96)

$$\frac{\bar{\rho}_{\text{vir}}}{\bar{\rho}(z_f)} = 18\pi^2 \varphi(z_f), \quad (1)$$

where the factor $\varphi(z_f)$ describes departures from a standard Einstein de-Sitter universe, and is given by

$$\varphi(z_f) \approx 1 + 0.4093W_f^{0.9052}, \quad (2)$$

where

$$W_f = 1/\Omega_f - 1, \quad (3)$$

$$\Omega_f = \frac{\Omega_0(1+z_f)^3}{\Omega_0(1+z_f)^3 + (1-\Omega_0-\Omega_\Lambda)(1+z_f)^2 + \Omega_\Lambda}. \quad (4)$$

In the above equations, $\bar{\rho}(z_f) = \Omega_0 \rho_{\text{crit},0} (1+z_f)^3$ is the mean matter density at redshift z_f , and Ω_0 and Ω_Λ are the present day densities of matter and cosmological constant, in units of the critical density $\rho_{\text{crit},0}$.

We assume that the cluster is isothermal, and that the gas acquires the virial temperature of the halo. In this case, the temperature is related to the mass and virial radius by the virial theorem,

$$\left(\frac{T_{\text{vir}}}{1 \text{ keV}} \right) \left(\frac{R_{\text{vir}}}{1 \text{ Mpc}} \right) = 0.88 \left(\frac{M_{\text{vir}}}{10^{14} M_\odot} \right), \quad (5)$$

where we have assumed that the gas has a mean molecular weight of $\mu = 0.59$, appropriate for a fully ionized mixture of H and He with a number density ratio of $n_{\text{He}}/n_{\text{H}} = 0.08$. Combining equations (1)–(5), the temperature of a cluster is given in terms of its mass and formation redshift,

$$\begin{aligned} \frac{T_{\text{vir}}}{[\text{KeV}]} &= 0.62(1+z_f) \left[\frac{\Omega_0 h^2}{0.17} \right]^{1/3} \\ &\times [\varphi(z_f)]^{1/3} \left(\frac{M_{\text{vir}}}{10^{14} M_{\odot}} \right)^{2/3} [\text{KeV}] \quad (6) \end{aligned}$$

Here $h \equiv H_0/100 \text{ km s}^{-1} \text{ Mpc}^{-1}$ is the Hubble constant. This equation quantifies the intuition that clusters virializing at an earlier epoch are hotter than clusters of the same mass that virialize at later times. Following KS96, we note that, in fact, clusters of a given mass M observed at a redshift z_o form over a range of earlier redshifts $z_f \geq z_o$. While equations (5-6) give the temperature and mass of a cluster when it first forms and virializes, the cluster is subsequently expected to evolve. In principle, both the mass and the temperature can change between z_f and z_o . As argued in KS96, numerical simulations (e.g., Evrard 1990, Navarro et al. 1995) indicate that the temperature does not significantly evolve after virialization. We therefore make the assumption here that the final temperature of the cluster at redshift z_o is equal to T_{vir} . Below, we will consider models that describe departures from this assumption (see § 2.3).

However, clusters do grow in mass after virialization. To account for this growth, we assume that the ratio between the final mass M and the mass at virialization M_{vir} is a “universal” constant $M_{\text{vir}} = f_M \times M$ for all clusters (see Lacey & Cole 1993; we will relax this assumption below). Following Viana & Liddle (1996), we set $f_M = 0.75$, which results in the best fit to the mass–temperature relation (both for its slope and scatter) in cluster simulations.

2.2. Mass Function and Age Distribution

The mass and formation redshift of a cluster are not directly measurable quantities. Nevertheless, it is possible to compute the cluster mass function, $dN/dM(M, z_o)$ (e.g., Press & Schechter 1974, Sheth, Mo & Tormen 1999, Jenkins et al. 2000), and also the statistical distribution of the formation redshifts z_f of clusters of a given mass M observed at redshift z_o , $dN/dz_f(M, z_o)$ (e.g., Lacey & Cole 1993, Sasaki 1994). In what follows, we will use the standard Press & Schechter (Press & Schechter 1974; PS) mass function, with fitting formulas for the cosmological transfer function (Sugiyama 1995), and for the critical overdensity $\delta_c(z)$ for collapse (KS96):

$$\begin{aligned} \delta_c(z) &= \delta_0(z)(1+z)g(0)/g(z) \\ \delta_0 &\simeq \frac{3(12\pi)^{2/3}}{20} (1 + 0.0123 \log_{10} \Omega_f). \quad (7) \end{aligned}$$

Here $(1+z)/g(z)$ is the usual linear theory growth factor (Peebles 1980). To obtain the formation redshift distribution for clusters of mass M at redshift z_o , we follow equation 2.26 in Lacey & Cole (1993; hereafter LC93), and define “formation redshift” as the redshift at which clusters first acquire a fixed fraction $f_M = 0.75$ of their final mass.

Our main motivation for the above choices is “technical”: the convenient semi-analytical derivation of dN/dz_f is only applicable to the mass function in the standard Press–Schechter theory; at present no analogous derivation exists for the improved mass functions, such as that of Jenkins et al. (2000). We also note that our qualitative conclusions below do not crucially depend on the shape of the distributions dN/dz_f and dN/dM . Nevertheless, it is important to emphasize that improvements over the PS mass function have already been made, and simulations have possibly uncovered differences in the abundance of massive clusters (e.g., Seth, Mo & Tormen 1999, Jenkins et al. 2000). Our analysis can be straightforwardly generalized to different choices for the mass function and formation redshift distribution, as the latter becomes available.

2.3. Deviations from Simple Spherical Collapse

The simple model described above assumes that clusters are fully virialized objects whose abundance and structure is dictated by gravitational physics alone. Lack of full virialization, on-going mergers, or feedback from galaxy formation can modify these predictions. For example, the above simple scaling relations, together with the assumption that the X-ray luminosity L_X is dominated by Bremsstrahlung emission, predicts $L_X \propto T^2$, while observations indicate the steeper relation $L_X \propto T^3$ (see, e.g., Kaiser 1991; Evrard & Henry 1991; Bryan & Norman 1998). Although different explanations are still possible (Bryan 2001) this steep slope suggests additional heat input to the gas prior to virialization, which preferentially lowers the central density, and therefore the X-ray emissivity, in smaller clusters (see, e.g., Kaiser 1991; Bialek, Evrard & Mohr 2001 and references therein for recent work on this subject).

To model deviations from our simplified model, we here introduce two additional parameters, ξ and α , by generalizing equation (6) as follows:

$$T_{\text{vir}} \propto (1+z_f)^\alpha M_{\text{vir}}^{1/\xi}. \quad (8)$$

The choice of $\xi = 1.5$ and $\alpha = 1$ corresponds to the original equation (6), while different values of ξ and α describe deviations from the simplest model. By design, both of these parameters capture departures from purely gravitational virial equilibrium (cf. eq. 5). The first parameter, ξ , mimics the effect of heat input. Preferential heating of small clusters corresponds to flattening the $T - M$ relation, i.e. to values of $\xi \geq 1.5$. This type of flattening has already been observed, e.g., $\xi \sim 1.6$ (Mohr & Evrard 1997), $\xi = 1.72$ (Muanwong et al. 2001; from analysis of cluster simulations), $\xi \simeq 1.81$ (Xu, Jin & Wu 2001), and $\xi = 1.98 \pm 0.18$ (Mohr, Mathiesen & Evrard 1999); 7%, 10%, 20%, and 25% variations respectively. Within the context of the spherical top hat model, this discrepancy is partly alleviated by the fact that smaller clusters form over a broader range of redshifts, and are on average hotter than larger cluster (which, on average, form closer to $z = z_o$). We find that the effective slope ξ_{eff} , under the assumption of $f_M = 0.75$, would be $\xi_{\text{eff}} \sim 1.6$. Nevertheless it is important to model possibly still larger deviations from the $\xi = 1.5$ scaling behavior.

The second parameter, α , quantifies deviations from the assumption that clusters at all redshifts are fully virialized. It is reasonable to consider, for example, the possibility that clusters at higher redshifts are more likely to be detected in the process of their initial collapse/assembly, and are less likely to be fully virialized than their lower-redshift counterparts. This effect is mimicked by a choice of $\alpha \leq 1$, implying cluster are “colder” at higher redshifts. Interestingly, there are examples of clusters hotter than one would expect if they were virialized (and can be taken as evidence for on-going mergers, or some other form of energy injection; e.g., Tucker et al. 1998, Roettiger, Loken & Burns 1997, Evrard, Metzler & Navarro 1996); this case is mimicked by a choice of $\alpha \geq 1$.

2.4. Modeling the Scatter

The model described above is “deterministic”: the only source of scatter it predicts in the observables is that caused by the fact that clusters have a distribution of different formation redshifts. This scatter is a direct consequence of cosmological initial conditions (which translates into a “scatter” by subsequent gravitational collapse), and probes the high- σ tail of the primordial power spectrum (Verde et al. 2000). For example, in the mass-temperature or size-temperature relations, this causes a scatter whose magnitude monotonically increases with decreasing temperature.

It appears that this scatter alone is sufficient to account for the scatter in the observed $M - T$ relation (Viana & Liddle 1996, Horner, Mushotzky & Scharf 1998, Finoguenov, Reiprich & Böhringer 2000, Xu, Jin & Wu 2001), and, for a suitable choice of σ_8 , for the observed scatter in the size-temperature relation (Verde et al. 2000, Mohr & Evrard 1997, Mohr et al. 2000). Nevertheless, it is interesting to contrast the predictions of this “cosmological” scatter with scatter that can be caused by different physics. For example, in a recent analysis of hydrodynamical cluster simulations (Mathiesen 2000), the X-ray temperatures do not appear to depend on the formation redshift (although see Evrard 1990 and Navarro et al. 1995, who find that cluster temperatures do not change after the cluster forms). These simulations are still inconclusive, since the expected correlation between formation redshift and cluster temperature is smaller than the scatter due to small-number statistics in the simulations. Furthermore, the observational scatter might even be due mostly to uncertainties in the mass, temperature (or size) determinations. We here nevertheless consider alternative origins for the scatter as a possibility.

We will distinguish two extreme cases as a *deterministic* scenario, in which the cluster temperature depends on the formation redshift, with no additional source of scatter; and a *stochastic* scenario, in which the temperature scales directly with the observed redshift, and there is some additional source of scatter. In the latter case, the additional scatter may simply be observational, or it may be caused by processes that influence cluster temperatures, such as feedback from galaxy formation, other forms of heating or cooling, or simply that f_M is not constant from cluster to cluster. Regardless of the source of this stochasticity, we assume that on average, the X-ray temperature of a cluster depends on its mass, redshift of observation and

cosmology through (6), with the substitution $z_f \rightarrow z_o$, but that there is, in addition, an intrinsic scatter around this mean $T(z_o)$ relation. We model this scatter as random deviations in the temperature from cluster to cluster, where the deviations ΔT are Gaussian distributed with a fractional *r.m.s.* width $x \equiv \Delta T/T$.

In reality, the scatter seen in cluster scaling relations is likely due to a combination of a deterministic effect (such as in our *deterministic* scenario) and a random variation from cluster to cluster (such as in the *stochastic* scenario). For example, as we will discuss in § 5.1 below, approximately the same scatter in the $M - T$ distribution could be obtained within the *deterministic* scenario (with $f_M = 0.75$; $x = 0$), or from a different scenario in which the formation redshift distribution was narrower (i.e. $f_M > 0.75$), but the cluster temperature had some additional random variation (i.e. $x > 0$). The parameter x , together with f_M , quantifies how much of the observed scatter is due to cosmological initial conditions *vs.* other sources. The *deterministic* scenario corresponds to ($f_M = 0.75$; $x = 0$); the *stochastic* scenario corresponds to ($f_M = 1$; $x > 0$); and in-between cases are described by ($f_M < 1$; $x > 0$).

2.5. Summary of Model Parameters

In principle, one would like to set all parameters of our model to be free, and investigate what joint constraint can be imposed from observations. However, the number of parameters makes this approach impractical, and we are forced to impose constraints using other observations. We assume the background cosmology to be a flat Λ cold dark matter (CDM) model (as supported by recent CMB data; Mauskopf et al. 1999, de Bernardis et al. 2000, Jaffe et al. 2000), described by the parameters Ω_0 and h . Unless otherwise stated, we will assume that the combination $\Omega_0 h^2$ is a constant (justified by the fact that forthcoming CMB experiments will constrain this combination to better than 5%). We also assume a baryon fraction $\Omega_b h^2 = 0.02$, consistent with recent D/H measurements (e.g., Burles & Tytler 1998). This leaves h as the only free cosmological parameter, and we will further impose $0.2 < h < 0.9$. The primordial power spectrum is specified by the normalization σ_8 and slope n ; however, we here assume $n = 1$ (supported by recent CMB data), and, unless otherwise stated, we also adopt $\sigma_8 = 0.495 \Omega_0^{-0.60}$ (inferred from local cluster abundance, Viana & Liddle 1999, Pierpaoli, Scott & White 2000).

In summary, our model is fully specified by the following 7 parameters:

- The cosmological parameters Ω_0 , h , and σ_8 ; two of which can be eliminated by other constraints.
- The parameters f_M and x that describe scatter in the scaling relations attributable to cosmological initial conditions, and to other sources, respectively
- The parameters ξ and α that describe departures from the fully virialized simple top-hat collapse models.

For illustrative purposes we define a “fiducial model” by the following choice of parameters: $h = 0.65$, $\Omega_0 h^2 = 0.17$,

$\Omega_0 = 0.4$, $\sigma_8 = 0.86$, $f_M = 0.75$, $x = 0$, $\xi = 1.5$, and $\alpha = 1$ for the *deterministic* model ; for the *stochastic* model we chose $x = 0.13$ and $f_M = 1$ and everything else remains unchanged. In addition to these parameters, to predict the Sunyaev–Zeldovich decrement (see § 3 below), we need to know the mass fraction of baryons that constitute the hot gas in the intra–cluster medium (ICM). This fraction (f_{ICM}) can be inferred from a comparison of the clusters X–ray flux and X–ray temperature; here we assume $f_{ICM} \sim 0.2$ with a weak temperature dependence: $f_{ICM} = 0.2T^{0.266}(h/0.5)^{-3/2}$ (Mohr, Mathiesen & Evrard 1999). We note here that the value of f_{ICM} should be a lower limit to the ratio Ω_b/Ω_0 ; the temperature dependence reflects the fact that low mass clusters are more likely to loose their gas from energy-injection or pre-heating mechanisms, while the dependence on h depends on the method employed to measure it. The method of Mohr et al. (1999) is a determination for the whole clusters, while the method of e.g., Grego et al. (2000b) yields a different h dependence but is based on the central SZ decrement. We have checked that the results we present here do not depend qualitatively on the specific choice of the dependence of f_{ICM} on h .

3. OBSERVABLES

The observables of a cluster that we utilize in this paper are the redshift (z_o), temperature (T), Sunyaev–Zeldovich total flux decrement (ΔS_ν), and angular size (θ). Within our model, the redshift and temperature are independent parameters and have already been specified. Cluster redshifts can be obtained observationally e.g., from their member galaxies out to $z_o \sim 1$ through deep optical and near infrared observations, and cluster temperatures can be obtained from X–ray spectra out to similar redshifts. Here we define the Sunyaev–Zeldovich decrement (SZD) and the angular size.

The SZD along a line of sight to a cluster in the Rayleigh-Jeans regime of the CMB is given by (e.g., Holder et al. 2000)

$$\frac{\Delta T_{CMB}}{T_{CMB}} = \frac{g k_B \sigma_T}{m_e c^2} \int dl n_e(l) T_e(l), \quad (9)$$

where $g = -2$, m_e is the electron rest mass, c is the speed of light, σ_T is the Thomson cross section, T_{CMB} is the CMB temperature, T_e is the electron temperature, n_e is the electron number density, and the integral is along the line-of-sight. Expressed in terms of a decrease in the observed flux, $\Delta S_\nu = 2k_B \Delta T_{CMB} \nu^2 / c^2 d\Omega$ (where $d\Omega$ is the smaller of the solid angle of the observations and the solid angle subtended by the cluster), equation (9) implies that the total observed SZ flux decrement (ΔS_ν) for a cluster can be related to its total mass via

$$\Delta S_\nu = \left(\frac{g 2 k_B^2 \nu^2 \sigma_T T_{CMB}}{\mu_e m_e m_p c^4} \right) f_{ICM} \frac{T_e M}{d_A(z)^2}, \quad (10)$$

where ν is the frequency, $\mu_e = 1.15$ is the mean molecular weight per electron, m_p the proton rest mass, d_A is the angular diameter distance, z is the cluster redshift, f_{ICM} is the ICM mass fraction and M denotes the mass enclosed within the virial radius of the halo. Equation (10) also

assumes that the electron density weighted mean temperature T_e can be identified with the virial temperature as given in equation (5) (this is satisfied by definition in our assumed isothermal clusters; we implicitly assume that T_e also equals the actual observed X–ray temperature T_X). Finally equation (10) assumes that the solid angle of the observations is larger than, or equal to the solid angle subtended by the cluster. Using equation (5), equation (10) can be rewritten in convenient units in terms of the observables z and T_X as:

$$\begin{aligned} \frac{\Delta S_\nu}{[\mu\text{Jy}]} &= 0.26(1+z_o) \left(\frac{\nu}{[\text{GHz}]} \right)^2 \\ &\times f_{ICM} \frac{M}{[10^{14} M_\odot]} \frac{T_X}{[\text{KeV}]} \frac{h^2}{d_A'^2} \end{aligned} \quad (11)$$

where we have introduced the dimensionless angular diameter distance $d_A' = d_A H_0 / c$, and z_o is the cluster redshift. The observable quantities here are z_o , T_X , and ΔS_ν .

In our model, the angular size of a cluster simply corresponds to the virial radius, $\theta = R_{vir}/d_A$. The spherically averaged profiles (of, e.g., temperature) found in numerical simulations do indicate the presence of a virialization shock, as expected from the top–hat collapse model. However, the shock tends to be weaker, and located at larger radii (see, e.g., Bryan & Norman 1998). Nevertheless, we here assume that the angular size is given by the virial radius, as obtained from the top hat collapse model (see further discussion below).

$$\frac{\theta}{[\text{deg}]} = \frac{\frac{\Delta S_\nu}{[\mu\text{Jy}]} f_M d_A'}{f_{ICM} 15.6(1+z_o) \left(\frac{\nu}{[\text{GHz}]} \right)^2 \left(\frac{T_X}{[\text{KeV}]} \right)^2 h} \quad (12)$$

Consistent with our earlier assumption, we have assumed that the cluster grows in mass by a factor of $1/f_M = 1.3$ between z_f and z_o . In practice, this angular size can be measured accurately only if a cluster is resolved, and therefore an estimate of θ will be available only for a fraction of the clusters in a dataset. For example, the Planck Surveyor satellite will resolve only about $\sim 1\%$ of all SZE clusters (Kay, Liddle & Thomas 2001), but the CSCS, with a 1.7' resolution, will resolve *most* clusters at $z \lesssim 1$ (Page et al. 2001). Angular sizes can, in principle, also be obtained from clusters resolved in X–ray observations. In practice, this involves measuring the profile and fitting to a model; this fit will be constrained essentially by the core radius, rather than the virial radius (although the latter can, of course, be inferred by extrapolation once the radial profile was fit to the model).

It is likely that in a given sample, not all observables will be known for each cluster, and the model prediction for some observables (e.g., for the angular size) are less robust than for others. Below, we will briefly consider the ideal case, in which all four observables ($z, T, \Delta S_\nu, \theta$) are reliably measured for a cluster sample. We will then concentrate on cases where only the subsets ($z, T, \Delta S_\nu$) or ($z, \Delta S_\nu, \theta$) have been measured. The first of these is relevant e.g., to a sample of clusters detected in the interferometric SZE survey of Holder et al. (2000), or to the MAP/Planck/CSCS cluster sample with X–ray follow-up and reliable temperatures; the second case is relevant to

a sample of well resolved SZE clusters (e.g., those of the CSCS) that are too distant ($z \gtrsim 1$) to obtain e.g., reliable temperatures. Current cluster samples exist where a combination of cluster sizes and temperatures are measured, and have been analyzed in the literature (see, e.g., Mohr & Evrard 1997, Verde et al. 2000).

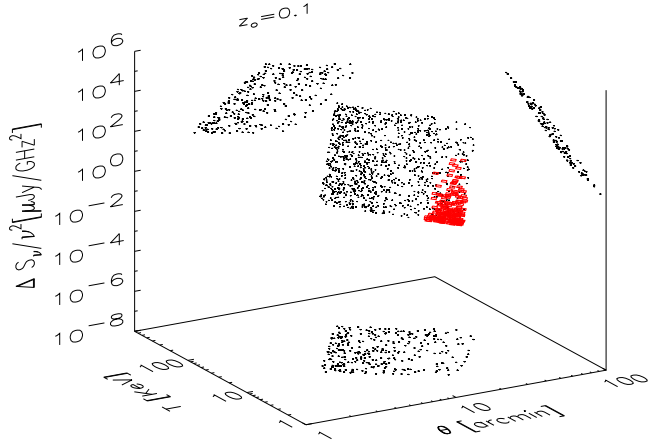


Fig. 1.— If clusters are standard candles, they populate a hypersurface in the 4 dimensional space of the observables (T_X , ΔS_ν , θ and z). Here, we show a slice of this space at the constant redshift $z_o = 0.1$. In this slice, clusters are constrained to be on a “fundamental plane”. The figure also shows the projection of this plane onto the “walls” of the box, defining the three scaling relations ($\Delta S_\nu - T_X$), ($\theta - \Delta S_\nu$), and ($\theta - T_X$). Not all locations in the fundamental plane are equally likely to be occupied: the filled symbols show the distribution of 200 Monte-Carlo generated clusters for our fiducial model. Deviations from the top-hat collapse model, or different choices of the cosmological parameters, cause measurable deformations of the FP such as a shift in its position and orientation, and can also introduce a random scatter around it.

4. THE FUNDAMENTAL PLANE OF GALAXY CLUSTERS

4.1. The Fundamental Plane in the Fiducial Model

At any given redshift z_o , the equations (6), (11) and (12) (i.e. in the *deterministic* scenario) express the three observables T_X , ΔS_ν and θ in terms of the two variables z_f and M . For a given frequency channel ν of the SZE survey, we assume that the ICM mass fraction has the functional form described in § 2.5 and that the cosmological parameters (Ω_0 , h , and σ_8) and f_M are known. These relations – three equations between the five variables (T_X , ΔS_ν , θ , M , and z_f) – allow a study of the distribution of clusters in several useful projections of this 5-dimensional parameter space. In particular, clusters define a 3-dimensional manifold in the 4-dimensional subspace of the four observables (T_X , ΔS_ν , θ , z). It is, however, more practical to consider the three dimensional subspace (T_X , ΔS_ν , θ), and regard the cluster redshift as an evolutionary parameter. In this case, for a given redshift z_o , clusters can only populate a half-plane in ($T_X, \Delta S_\nu, \theta$)-space. The restriction to a half-plane arises from the requirement that clusters form prior to the redshift at which they are observed, $z_f \geq z_o$.

In order to visualize this half-plane, which we will hereafter refer to as the “fundamental plane” (FP), in Figure 1

we show an example of the distribution of clusters observed at the fixed redshift $z_o = 0.1$. The figure also shows the projection of the FP onto the “walls” of the box, which define the three scaling relations ($\Delta S_\nu - T_X$), ($\theta - \Delta S_\nu$), and ($\theta - T_X$). Of course, not all locations in the FP are equally likely to be occupied: cluster temperatures, virial radii and SZ decrements cannot assume any arbitrary value between $-\infty$ and $+\infty$; smaller clusters are more numerous than high temperature ones; and the width of the probability distribution of z_f decreases monotonically for larger clusters. As a result, clusters preferably populate a portion of the FP. In Figure 1, the filled symbols show the distribution of 200 clusters, selected randomly at $z_o = 0.1$ using a Monte-Carlo method.

If all observable quantities T_X , ΔS_ν , θ and z are measured in a cluster sample, and the top hat collapse model is the correct description of the physical properties of clusters, then the clusters define the FP shown in Figure 1, determined solely by the cosmological parameters. Deviations from the top-hat collapse model, or different choices of the cosmological parameters, can cause a shift in the position and orientation of the FP, and can also introduce a random scatter around it. We will argue that it is possible to quantify such deviations from the simple top-hat model, and gain insight into both cluster physics and cosmological parameters, by studying the departures of the FP from its position and orientation in our “fiducial” model. As an example, $\alpha < 1$ would modify the dependence of the FP on redshift z ; while $x > 0$ would induce a scatter around the FP. In the rest of this paper, we will quantify these statements, by concentrating on different projections of the FP.

4.2. The Fundamental Plane and Cluster Scaling Relations

As mentioned above, the projections of the FP define three scaling relations, ($\Delta S_\nu - T_X$), ($\theta - \Delta S_\nu$), and ($\theta - T_X$). The last of these relations can be analyzed using existing cluster samples, and have been studied by various authors (e.g., Mohr & Evrard 1997, Verde et al. 2000). In this paper, we focus on the usefulness of the first two scaling relations, which will be observationally available from future SZE cluster surveys.

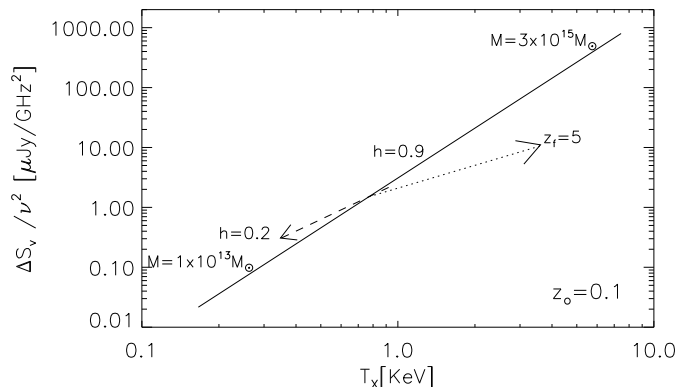


Fig. 2.— Theoretical expectations for the projection of the fundamental plane defining the ($\Delta S_\nu - T_X$) scaling

relation. The solid line shows the location of clusters in our fiducial model at redshift $z_o = 0.1$ with masses between $10^{13} M_\odot \leq M \leq 3 \times 10^{15} M_\odot$, assuming that they formed at the redshift at which they are observed, $z_f = z_o = 0.1$. The dotted arrow shows how the location of a $2 \times 10^{14} M_\odot$ cluster depends on its formation redshift for $0.1 < z_f < 5$. Similarly, the dashed arrow shows how the location of this cluster would change with the Hubble constant for $0.2 < h < 0.9$. Changes in Ω_0 or σ_8 mainly affect how the clusters are distributed in the direction of the dotted arrow. Note that this arrow is nearly parallel to the solid line; this suggests that the scatter in the $(\Delta S_\nu - T_X)$ should be small.

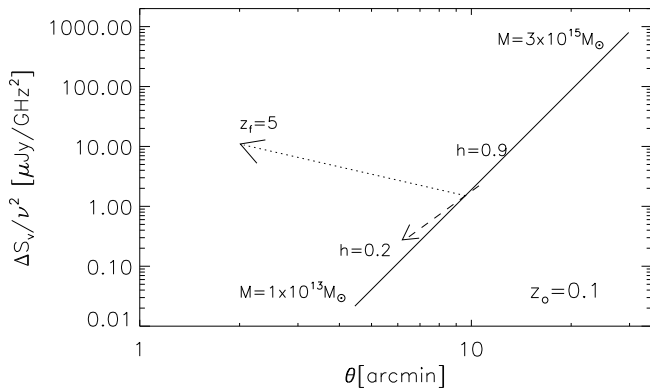


Fig. 3.— Theoretical expectations for the projection of the fundamental plane defining the $(\Delta S_\nu - \theta)$ scaling relation. The solid line, and the dotted and dashed arrows describe the same clusters as in Figure 2. Note that in difference from Figure 2, the dotted arrow, representing increasing formation redshifts, is nearly orthogonal to the solid line. This suggests that the scatter in the $(\Delta S_\nu - \theta)$ should be large, and sensitive to Ω_0 , σ_8 and primordial non-gaussianity (the same conclusion holds for the size–temperature relation, as can be seen from Figure 1; see also Verde et al. 2000).

Figures 2 and 3 show the theoretical expectations for the two projections of the FP that involve the Sunyaev–Zeldovich decrement, together with the expected position of clusters in our fiducial model. Figure 2 shows the projection of the FP onto the $(\Delta S_\nu - T_X)$ plane. The solid line shows the location of clusters at redshift $z_o = 0.1$ with masses between $10^{13} M_\odot \leq M \leq 3 \times 10^{15} M_\odot$ in this plane, assuming that these clusters formed at the redshift at which they are observed, $z_f = z_o = 0.1$. The dotted arrow shows how the location of a $2 \times 10^{14} M_\odot$ cluster in this plane depends on its formation redshift for $0.1 < z_f < 5$. As the arrow demonstrates, both the temperature and SZD are increased for clusters that form earlier. Similarly, the dashed arrow shows how the location of this cluster would change with the Hubble constant for $0.2 < h < 0.9$. Both the temperature and SZD decrease if the Hubble constant is lower. Note that changes in Ω_0 and σ_8 mainly affect how clusters are distributed in formation redshift, i.e. along the direction of the dotted arrow. Since this is nearly parallel to the solid line, a change in Ω_0 or σ_8 is nearly degenerate with a change in cluster mass.

This suggests that the expected scatter in the $(\Delta S_\nu - T_X)$ relation should be small, and insensitive to Ω_0 and σ_8 . Notice also that low values of h make clusters appear colder, mimicking an unphysical formation redshift $z_f < z_o$.

Figure 3 shows the projection of the FP onto the $(\Delta S_\nu - \theta)$ plane. As in Figure 2, the solid line shows the location of clusters at redshift $z_o = 0.1$ with masses between $10^{13} M_\odot \leq M \leq 3 \times 10^{15} M_\odot$, while the dotted and dashed arrows demonstrate the dependence of the location of a $2 \times 10^{14} M_\odot$ cluster on its formation redshift and on the Hubble constant. Note that in difference from Figure 2, the dotted arrow, representing increasing formation redshifts, is nearly orthogonal to the solid line. This suggests that the scatter in the $(\Delta S_\nu - \theta)$ should be large, and sensitive to Ω_0 , σ_8 and primordial non-gaussianity. The same conclusion holds for the size–temperature relation, as can be seen from Figure 1 (see also Verde et al. 2000).

5. PROBING THE INTERNAL PHYSICS OF CLUSTERS

The idealized model for clusters described in § 2.1 is based on the collapse of a spherical top hat perturbation, and is the simplest model to relate cluster observables. It is important to have observational tests for departures from this model; both in order to understand the structure of clusters themselves, and also to allow clusters to be used as “standard candles” in cosmological studies. As discussed above, all four observables $(\Delta S_\nu, T, z, \theta)$ might not be available for every cluster. This prompts us to consider what constraints are possible both with and without knowing the angular size θ . In this section we will assume that cosmological parameters are known and use the deformations of the FP to test whether clusters are “standard candles”.

5.1. Testing for the Origin of Scatter

A striking feature of the FP in our fiducial model, shown in Figure 1, is its orientation, which implies that the three projections have significantly different scatter. In particular, a relatively large scatter is predicted around the $(\theta - \Delta S_\nu)$ and $(\theta - T_X)$ scaling relations, while the $(\Delta S_\nu - T_X)$ relation remains much more tightly defined. Figures 2 and 3 reveal that this result follows from the deterministic nature of our fiducial model, where the only source of scatter in the observables is the distribution in formation redshift z_f of clusters (which, ultimately, is a direct consequence of cosmological initial conditions). As discussed in § 2.4 above, the deterministic scenario, without any additional sources of scatter, might be consistent with existing data (i.e. the scatter in the $\theta - T_X$ and $M - T_X$ relations). Nevertheless, it is interesting to consider alternative options, those in-between the two extreme *deterministic* and *stochastic* scenarios.

The parameters x , and f_M , introduced in § 2.4 above, quantify how much of the observed scatter is caused by cosmological initial conditions, or by random variations from cluster to cluster, arising from their internal physics. To quantify this we Monte–Carlo generate the $M - T$ relation of a mock catalog of about 250 clusters, first in our deterministic fiducial model with $(f_M = 0.75, x = 0)$, and then for different combinations of f_M and x . We then

compare those to the fiducial model with a 2 dimensional Kolmogorov-Smirnov test (e.g., Press et al. 1992, Peacock 1983, Fasano & Franceschini 1987). This test computes the D statistic, that is the maximum cumulative difference between the two distributions, and then gives $P_{>D}$, the probability that D could be greater than observed. Small values of $P_{>D}$ indicate that it is extremely likely that the two distributions differ, for example a conservative choice is usually $P_{>D} < 0.01$ which implies that the two data sets are significantly different. We have checked with multiple realizations that if two datasets are drawn from the same underlying distribution (i.e. our fiducial model) $P_{>D} > 0.317$ about 68% of the times and $P_{>D} > 0.046$ about 95% of the times. In what follows we will thus plot the equal probability contours corresponding to $P_{>D} = 0.317, 0.046$ and 0.01 .

Figure 4 show these equal probability contours. Note that the *deterministic* scenario corresponds to ($f_M = 0.75; x = 0$); the *stochastic* scenario corresponds to ($f_M = 1; x > 0$); and in-between cases are described by ($f_M < 1; x > 0$).

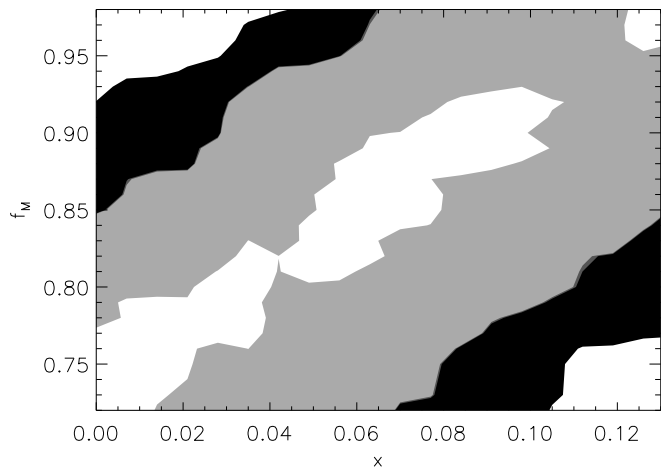


Fig. 4.— We illustrate a probabilistic study of the origin of the scatter in the $M - T_X$ relation. The scatter can arise from cosmological initial conditions ($f_M = 0.75, x = 0$), or from a stochastic source ($f_M = 1$). Other choices of (f_M, x)-values correspond to a combination of both effects. The equal-probability contours for $P_{>D} = 0.317, 0.046, 0.01$, where $P_{>D}$ is the likelihood that the two data sets are drawn from the same distribution, are shown in the f_M - x plane. The likelihoods were obtained from a 2D Kolmogorov-Smirnov (KS) test of the $M - T_X$ distribution of 250 clusters at redshift $z = 0$. Probabilities are obtained by comparing the $M - T_X$ distributions to that in our fiducial flat Λ CDM model with $f_M = 0.75$ and $x = 0$. The parameter space outside the light gray area is excluded by the KS test at $\sim 68\%$ confidence.

Figure 4 has two important implications. First, the parameter space outside the light gray area is excluded by the KS test at the 68% confidence level ($P_{>D} < 0.317$), indicating that the $M - T_X$ relation by itself can already be a useful discriminant for the source of scatter. Forthcoming datasets can yield a local sample of many more than 250 clusters with size, temperature, and mass estimates, in which case the constraints shown in Figure 4 can be signif-

icantly improved. Second, Figure 4 suggest that although their combination is tightly constrained from the $M - T_X$ distribution alone, a degeneracy appears to still remain between f_M and x . A comparison with Figure 1 suggest that this degeneracy can be broken by considering, in addition, the distribution of clusters along the $\Delta S_\nu - T_X$ relation. For models where the scatter is cosmological ($f_M \approx 0.75$), this relation is significantly tighter than the $\theta - T_X$ distribution. On the other hand, in “stochastic” models ($f_M \approx 1$), the scatter in $\Delta S_\nu - T_X$ should be comparable to that in $M - T_X$.

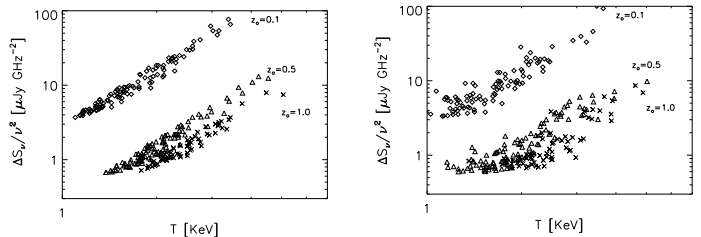


Fig. 5.— The distribution of 100 Monte Carlo clusters in the $\Delta S_\nu - T_X$ plane. Clusters were selected with masses above $10^{14} h^{-1} M_\odot$, observed at redshifts $z_o = 0.1$ (diamonds), $z_o = 0.5$ (triangles), and $z_o = 1$ (crosses). The left panel corresponds to our fiducial model, in the *deterministic* scenario, where the scatter is purely from cosmological initial conditions. The right panel shows the *stochastic* scenario, with a stochastic scatter. Although both scenarios, by construction, have the same scatter in the $M - T_X$ relation, the stochastic scenario predicts a significantly larger scatter in $\Delta S_\nu - T_X$ than the deterministic one.

We therefore next examine constraints on (f_M, x) that will be available from clusters with measured z and ΔS_ν . In order to illustrate how the scatter in the $\Delta S_\nu - T_X$ relation differs in the stochastic and deterministic scenarios, in Figure 5 we show the distribution of clusters in this plane. We used Monte-Carlo realizations of our fiducial model to generate a catalog of ~ 100 clusters with masses above $10^{14} h^{-1} M_\odot$ (cf. Holder et al. 2000), observed at each of the redshifts $z_o = 0.1, 0.5$, and 1 .

The left and right panels of Figure 5 show the distributions in the deterministic and stochastic scenarios, respectively. A comparison of the two panels reveals that at any redshift, the scatter in the deterministic scenario is small; while in the stochastic scenario, it is significantly larger. We find that the two scenarios differ increasingly towards higher redshifts. This is not surprising, since in the deterministic scenario, the scatter is reduced by the narrower distribution of cluster ages at high- z , while in the stochastic scenario, there is no similar trend.

In what follows, we find it useful to define a combination η of the observables ($\Delta S_\nu, T, z$) by

$$\eta \equiv \frac{2.45 \times 10^{-4} (T_X / [KeV])^{5.532}}{(1+z) \Omega_0 \wp(z) (\frac{\Delta S_\nu}{\nu^2} / [\mu Jy / GHz^2]) f_M d_A^2} \quad (13)$$

Under the assumption that a cluster at redshift z formed at the same redshift $z_f = z$, η would simply equal the Hubble constant $\eta \equiv h$. In general, for a sample of clusters with different ages, $\eta \geq h$ since $z_f \geq z$. As a result, in our fiducial model (*deterministic* scenario), for any given

redshift or temperature, the lowest value of η (η_{min}) in a cluster sample gives an estimate of h . In the left panel of Figure 6), we show the distribution of clusters in the $\eta - z$ plane. Inadequacies of our fiducial model will show up as a systematic dependence of h (η_{min}) on z (and/or on T_X ; see further discussion below).

We next quantify how the combination η , defined in equation (13), depends on z and T_X in different models. We generate a Monte-Carlo mock catalog of ~ 300 clusters between redshift $0 \leq z \leq 1$ in our fiducial model. We impose the restriction $z \leq 1$ because of the increasing difficulty to obtain accurate cluster redshifts for more distant clusters. The survey proposed by Holder et al. (2000) will yield about 300 clusters with $z \lesssim 1$. Similarly, in the CSCS survey proposed by Page et al. (2001), about ~ 300 of the detected SZE clusters will have redshifts measured in X-rays and/or optical follow-up observations. For each cluster in our mock catalog, we then compute η , using equation (13).

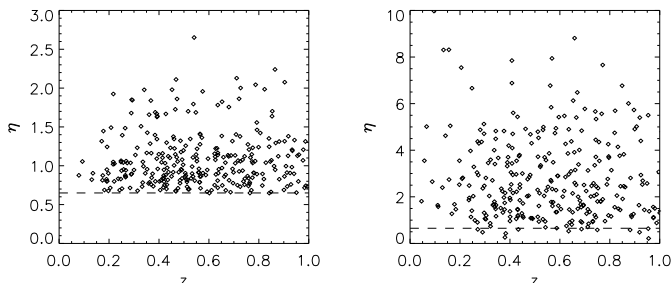


Fig. 6.— Scatter plot of η from Monte Carlo simulations of ~ 300 clusters. The true underlying cosmological parameters are those for our fiducial model ($\Omega_0 = 0.4$, $\Lambda_0 = 0.6$, $h = 0.65$). The horizontal dashed line show where clusters for which $z_o = z_f$ should lie. The left panel corresponds to our *deterministic* fiducial model, while the right is for the *stochastic* model. Note the different scale in the y axis and the different distributions of points relative to the dashed line.

Using these Monte-Carlo catalogs, we can now determine constraints on (f_M, x) . We compare mock catalogs of ~ 300 clusters, assuming different combinations of (x, f_M) in otherwise identical models. Instead of using the deterministic scenario for the benchmark model, we adopt $f_M = 0.85$ and $x = 0.065$. This combination lies approximately in the center of the degenerate parameter range shown in Figure 4, and hence it allows us to quantify the “distance” of both deterministic and stochastic scenarios from this intermediate case. The $P_{>D} = 0.317, 0.046$, and 0.01 probability contours obtained from these KS tests are shown in Figure 7.

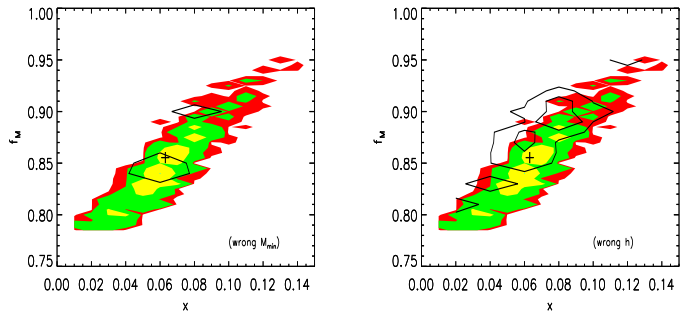


Fig. 7.— Equal probability contours at $P_{>D} = 0.317, 0.046$ and 0.01 in the (x, f_M) plane, obtained from 2D KS tests between distributions of the clusters in the (η, z) plane. Each pair of (x, f_M) was used to generate a mock catalog of 300 clusters, and its (η, z) distribution was compared to that in a benchmark model with $f_M = 0.85$ and $x = 0.065$. The parameter space outside the light gray area is excluded by the KS test at 68% confidence. The two sets of transparent contours show $P_{>D} = 0.317$ and $P_{>D} = 0.046$ (nominally 68.3% and 95.4% respectively) contours obtained by generating mock catalogs down to a factor 2 lower value of M_{min} than in the fiducial model (left panel); or similarly, assuming the wrong value of h by +5% (right panel). Larger errors on M_{min} or h would imply that no combination of (x, f_M) produces a (z, η) distribution consistent with our fiducial model.

The shaded contours (identical on both panels) reveal that tight constraints can be derived on a combination of (x, f_M) , similar, but not identical to those from the $M - T$ relation. In using these types of constraints, it is important to compare observational data with model catalogs extending down to the “correct” minimum mass, i.e. the true mass of the smallest observed cluster. The shaded confidence regions were obtained by implicitly assuming the right minimum mass (M_{min}) of the survey. To demonstrate the sensitivity of this method to the limiting mass, in the left panel of Figure 7, the set of transparent contours shows $P_{>D} = 0.317, 0.046, 0.01$, obtained assuming a value for M_{min} that is too low by a factor of two. Similarly, the transparent contours in the right panel show the results we obtain if we assume the wrong value of h by +5%. A larger error on these two parameters would result in all combinations of (x, f_M) producing a (z, η) distribution that is inconsistent with the distribution in our benchmark model. This conclusion does not change if we reverse the sign of the change in M_{min} and h . This suggests that this type of study can be used to simultaneously constrain (x, f_M) , as well as M_{min} and h . Our results in Figure 7 also suggest that if one marginalizes over the allowed ranges of M_{min} and h , the errors on x and f_M will not be significantly increased.

5.2. Cluster Evolution and Feedback

In § 2.3 we introduced two parameters that describe deviations arising from energy injection, or other feedback (ξ); and from lack of full-virialization, or redshift-evolution due to other reasons (α). In our fiducial model, $\xi = 1.5$ and $\alpha = 1$. It is interesting to quantify the effects on the cluster scaling relations of different choices for both

parameters. As suggested in the previous section, an inadequacy in our fiducial model will show up as a systematic dependence of η (eq. 13) on z and/or T_X . For example, a 20% variation in the value of ξ has a sizeable effect in the distribution of η vs T , as we demonstrate in the right panel of Figure 8.

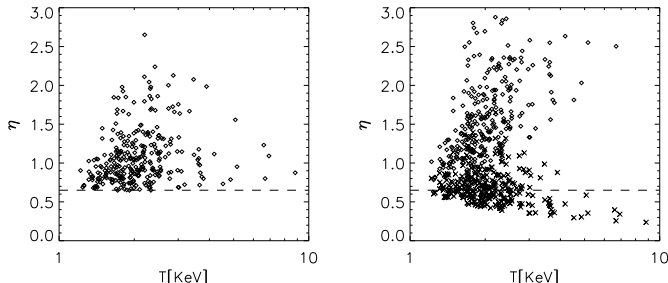


Fig. 8.— Scatter plot of η from Monte Carlo simulations of ~ 300 clusters. The true underlying cosmological parameters are those for our fiducial model ($\Omega_0 = 0.4$, $\Lambda_0 = 0.6$, $h = 0.65$). The horizontal dashed line show where clusters for which $z_o = z_f$ should lie. The left panel corresponds to our *deterministic* fiducial model, while in the right panel the parameter ξ in the scaling relation (eq. 6) has been changed from the fiducial value $\xi = 1.5$ to $\xi = 1.8$ (diamonds) and $\xi = 1.2$ (crosses).

In this figure, we show η vs. T for $\xi = 1.5$ (left panel), and for $\xi = 1.8$ (right panel; diamonds) and $\xi = 1.2$ (right panel; crosses), in the fiducial model.

In order to quantify the minimal level of deviations that can be measured in future SZE surveys, we performed a 2D KS test in the $\eta - z$ distribution for the α parameter using Monte Carlo simulations of 300 clusters. We find that deviations from $\alpha = 1$ by ± 0.03 are detectable at 68% confidence level. Performing the same test in the $\eta - T_X$ plane for the ξ parameter, we find deviations from the value $\xi = 1.5$ by $\xi = 1.5^{+0.02}_{-0.05}$ are detectable at the same significance.

If angular sizes of ~ 300 clusters in a survey are available, in addition to $(\Delta S_\nu, T, z)$, the values of x , f_M and cosmological parameters can be accurately determined. From equation (12) we obtain:

$$\frac{h}{d'_A} = \frac{\frac{\Delta S_\nu}{[\mu\text{Jy}]} f_M}{(\frac{\nu}{[\text{GHz}]})^2 f_{\text{ICM}} (\frac{T_X}{[\text{KeV}]})^2 \frac{\theta}{[\text{deg}]} (1 + z_o) 15.6} \quad (14)$$

If we consider this combination of observables as a function of z_o , we find that (a) the scatter around this relation is not sensitive to f_M , and hence it can only be due to a non-zero value for the parameter x ; and (b) the absolute normalization of the relation depends on the angular diameter distance and f_M . In particular, if cosmological parameters are known, the latter depends only on f_M .

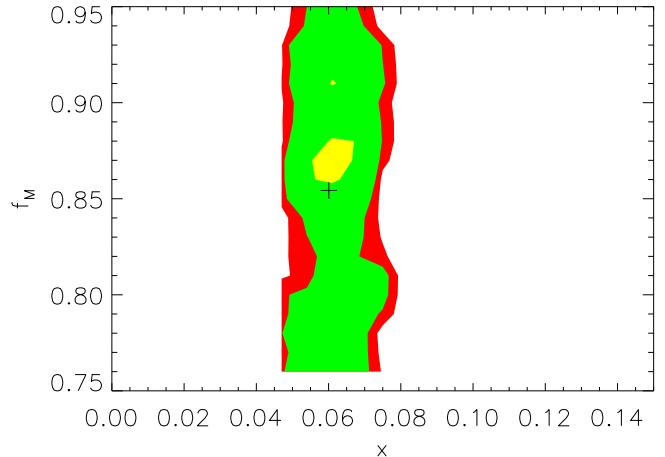


Fig. 9.— Equal probability contours at $P_{>D}=0.317$, 0.046 and 0.01 in the (x, f_M) plane, obtained from 2D KS tests between distributions of the clusters using the combination of four observables as in equation (14) as a function of z_o . The combination of these contours with those of Figure 7, allows a unique combination of (x, f_M) to be determined.

These properties of the combination of observables in equation (14) allows a unique combination of (x, f_M) to be measured. Figure 9 shows the equal probability contours ($P_{>D}=0.317$, 0.046, 0.01) in the $f_M - x$ plane for a sample of 300 clusters: the “product” of the probability contours of Figures 7 and 9 allows a unique combination of (x, f_M) to be determined. In addition, the redshift dependence of equation (14) directly probes the redshift evolution of the angular-diameter distance, and therefore can be further utilized to measure cosmological parameters, as we will discuss in § 6.3.

6. PROBING COSMOLOGICAL PARAMETERS

In this section, we will assume that clusters can be used as standard candles, i.e. that our modeling of cluster physics is accurate. The deformations of the FP relative to its shape in the fiducial model can then be used to determine cosmological parameters.

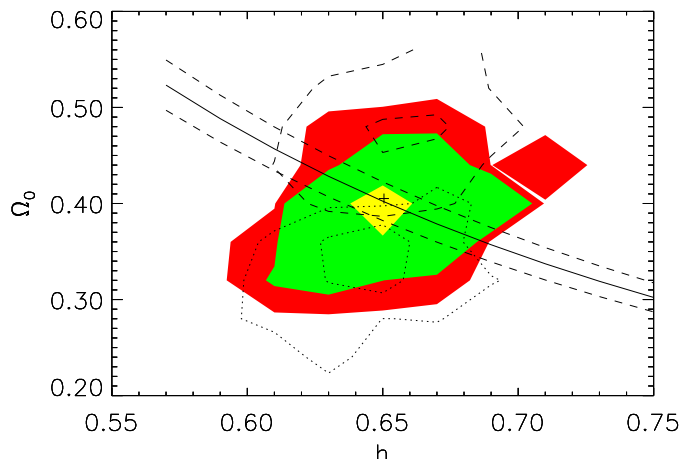


Fig. 10.— Equal probability contours in the $(h - \Omega_0)$ plane obtained from the 2D KS test of the $\eta - z$ distribution, similar to those shown in Figure 6. The parameter

space outside the light gray area is excluded by the KS test at the $\sim 68\%$ level ($P_{>D} = 0.317$), the other two contours correspond to $\sim 95\%$ and $\sim 99\%$ confidence levels. The “true” underlying value is indicated by the cross. The dotted and dashed contours show the first two likelihood contours ($P_{>D} = 0.317$ and 0.046), obtained by assuming a minimum mass for the survey M_{\min} two times lower and two times higher than the $10^{14}h^{-1} M_{\odot}$ used in the mock catalog. The estimates of h are not strongly affected by the choice of M_{\min} . In practice, one will marginalize over M_{\min} : this will increase the uncertainty in the recovered Ω_0 , but not in h . The solid line, together with the two dashed lines, show the constraint $\Omega_0 h^2 = \text{constant}$, and $\pm 5\%$ uncertainties, expected from forthcoming CMB experiments.

6.1. Constraints from $\Delta S_{\nu}, T$, and z .

Assuming only ΔS_{ν} and T_X and z_0 are available, a 2D KS test applied to the $\eta - z$ distribution (see Figure 6), can be used to constrain Ω, h . It is important to note here that this measurement of the Hubble constant, based on a combination SZE and X-ray data, is different from an existing method proposed by e.g., Gunn (1978), Silk & White (1978), Birkinshaw (1979). The latter method, by combining the central SZ decrement with X-ray central temperature, yields an estimate of the length of the cluster; assuming that the cluster is spherical this can be used as an angular diameter distance test. By averaging over a large cluster sample, effects of cluster asphericity can be averaged out. In this method clusters are used as *standard rulers*. The method presented here is complementary; it uses the total observed SZ flux decrement, which can be directly measured, requires data that is easier to obtain (no detailed SZ and X-ray map of the cluster are needed) and by making use of the whole cluster SZD, should therefore be less sensitive to the details of cluster physics near the center. This method relies on different assumptions; it assumes clusters are virialized (although deviations from virialization can be parameterized, as discussed in § 2.3 and 2.4). In our method, clusters are used as *standard candles*. The expected statistical errors for a cluster sample of the same size are comparable for the two methods, but the possible systematics are of entirely different nature.

Results of the 2D KS test of the $\eta - z$ distribution of Ω, h are shown in Figure 10. The parameter space outside the light gray area is excluded by the KS test at the 68% level ($P_{>D} = 0.317$), the other two contours correspond to $P_{>D} = 0.046$ and $P_{>D} = 0.01$. The “true” underlying value is indicated by the cross. The dotted and dashed contours show the first two likelihood contours ($P_{>D} = 0.317$ and 0.046), obtained by assuming a minimum mass for the survey M_{\min} two times lower and two times higher than the $10^{14}h^{-1} M_{\odot}$ used in the mock catalog. The estimates of h are not strongly affected by the choice of M_{\min} . In practice, one will marginalize over M_{\min} : this will increase the uncertainty in the recovered Ω_0 , but not in h . The solid line, together with the two dashed lines, show the constraint $\Omega_0 h^2 = \text{constant}$, and $\pm 5\%$ uncertainties, expected from forthcoming CMB experiments. This suggests that the two constraints are suf-

ficiently different, and can be combined together to break the degeneracy between Ω_0 and h .

6.2. Constraints from $\Delta S_{\nu}, \theta$, and z .

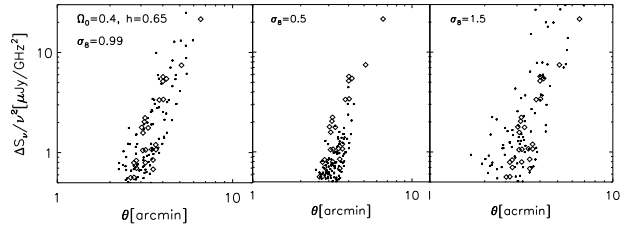


Fig. 11.— The dependence of the $\Delta S_{\nu} - \theta$ distribution on σ_8 ($\Delta S_{\nu}/\nu^2$ is in units of $\mu\text{Jy}/\text{GHz}^2$). The diamonds show a Monte Carlo sample of 25 clusters at $z = 0.3$ with $\theta \gtrsim 2'$ (close to the specifications of the CSCS survey) for $\Omega_0 = 0.3$, $\Lambda_0 = 0.7$, $h = 0.65$ and $\sigma_8 = 0.99$; the dots show the $\Delta S_{\nu} - \theta$ distribution of ~ 100 Monte-Carlo simulated clusters for different choices of σ_8 .

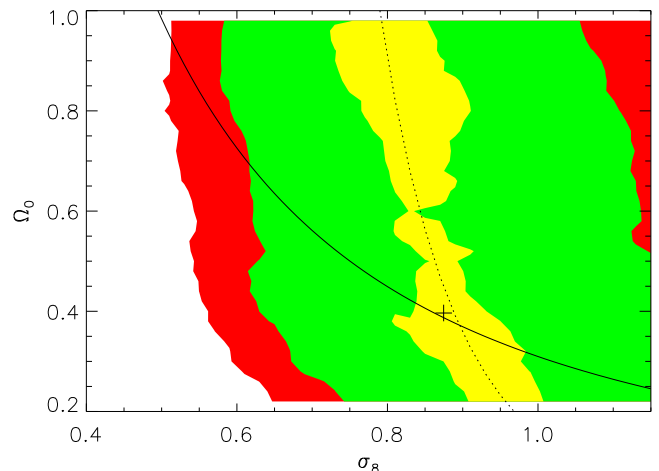


Fig. 12.— Equal probability contours in the $\sigma_8 - \Omega_0$ plane, obtained from the $\Delta S_{\nu} - \theta$ relation. The parameter space outside the light gray area is excluded at the 68% ($P_{>D} = 0.317$) level by the KS test. The constraint we obtain can be approximated by $\sigma_8 = 0.92\Omega_0^{-0.11}$. For reference, the solid line shows the constraint in the $\sigma_8 - \Omega_0$ plane obtained from the local abundance of massive clusters. A comparison suggests that the two constraints can be used together to measure Ω_0 and σ_8 simultaneously.

Assuming that clusters in the sample are resolved, and that their angular sizes (θ) are measured, a 2D KS test applied to the $\Delta S_{\nu} - \theta$ distribution (see Figure 11), can be used to constrain Ω_0 and σ_8 . In Figure 11, we illustrate the dependence of the $\Delta S_{\nu} - \theta$ distribution on σ_8 ($\Delta S_{\nu}/\nu^2$ is in units of $\mu\text{Jy}/\text{GHz}^2$). The diamonds show a Monte Carlo sample of 25 clusters at $z_0 = 0.3$ with $\theta \gtrsim 2'$ for $\Omega_0 = 0.4$, $\Lambda_0 = 0.6$, $h = 0.65$ and $\sigma_8 = 0.99$; the dots show the $\Delta S_{\nu} - \theta$ distribution of ~ 100 Monte-Carlo simulated clusters for different choices of σ_8 . It is clear that a too large/small σ_8 gives rise to a too large/small scatter in the $(\Delta S_{\nu} - T)$ relation.

The results are demonstrated in Figure 12, where we show the equal probability contours in the $\sigma_8 - \Omega_0$ plane

obtained from the $\Delta S_\nu - \theta$ relation. The fiducial model is indicated by the cross (here we have dropped the constraint $\sigma_8 = 0.495\Omega_0^{-0.6}$). As before, the parameter space outside the light gray area is excluded at the 68% level by the KS test, and the other two sets of contours correspond to 95% and 99% confidence levels. The constraint obtained from the $\Delta S_\nu - \theta$ relation can be approximated by $\sigma_8 = 0.92\Omega_0^{-0.11}$. For comparison, the solid line shows the constraint in the $\sigma_8 - \Omega_0$ plane obtained from the local abundance of massive clusters. A comparison of these two methods suggests that the two constraints can be used together to measure both Ω_0 and σ_8 .

6.3. Constraints from $\Delta S_\nu, \theta, T$ and z .

As already mentioned in § 5.2 above, if all observables are known for a cluster sample, and if f_M and x are reasonably well constrained, then equation (14) yields the angular diameter distance as a function of redshift. This quantity depends on Ω_0, Λ, h and the equation of state parameterized by w ; it can thus be used to constrain these parameters. Several other observables have already been used to measure the angular diameter distance as a function of redshift, such as type Ia supernovae (e.g., Reiss et al. 1998; Perlmutter et al. 1998) or the redshift evolution of the linear power spectrum shape (e.g., McDonald & Miralda-Escude 1999; Roukema & Mamon 2000). Galaxy clusters potentially offer an independent test. The accuracy with which the angular diameter distance can be measured will strongly depend on the observational uncertainties in $\Delta S_\nu, \theta$ and T and will be addressed in a subsequent work.

7. A COMPARISON OF TWO DIFFERENT STATISTICS

Throughout this paper, we have adopted the 2D KS test to quantify the discriminating power of the scaling relations between different models. In our study, we have focused on the *shapes* of the scaling relations, and have not explored constraints from the *total number* of detected clusters, which itself is a function of cosmological parameters. The cosmology dependence of the number counts has been recently studied by Haiman, Mohr & Holder (2001) and Holder, Haiman & Mohr (2001) to forecast precision-constraints that will be available on the equation of state parameter w , as well as the parameters Ω_0, Ω_Λ , and σ_8 . These constraints are complementary to those that derive from the shape of the scaling relations, and the two methods will have different systematic errors. For example, the fundamental plane approach requires extensive X-ray/optical follow-up of SZ surveys, or requires the temperatures of SZ selected clusters to be obtained from different catalogs. This can introduce selection effects which affect the number of detected clusters, but not the shape of the scaling relations. The KS test has several attractive features, such as its distribution independence and the fact that is a robust and more direct method. It is a particularly appropriate statistic for the present application, since it distinguishes distributions based only on their shape, independent of their overall normalization. Nevertheless, one must bear in mind that the KS test is optimized to detect “shifts” in distributions, and is less well-suited in distinguishing among distributions with significant “tails”

(e.g. Press et al. 1992). In order to assess the robustness of our results to the choice of statistic, we here compare our analysis of the constraint on the Hubble constant h with constraints obtained from a maximum likelihood method. In applying both types of statistic, we utilize the distribution of clusters in the $(\eta - z_o)$ plane, as defined in § 5.1 above, to derive constraints on the Hubble constant.

In general, a maximum likelihood analysis is not directly comparable to the KS test, since the former utilizes information from the total number of clusters, while the latter is insensitive to it. However, in the case of constraining the Hubble constant, we find that the total number of clusters is insensitive to the value of h . As an example, in our fiducial model with $h = 0.65$, we predict, by construction, 300 clusters between redshifts $0.1 < z < 1$, in a solid angle of $\sim 20 \text{ deg}^2$, above the limiting mass $M_{\min} = 10^{14} h^{-1} M_\odot$. Assuming that the minimum mass M_{\min} scales as $M_{\min} \propto h^{-1}$ (e.g. from mass determinations from X-ray profiles, weak lensing, etc.), and assuming further that the power spectrum has been independently measured, we find that the total count is essentially independent of h . Lack of a-priori knowledge of the power spectrum introduces a small h -dependence through the “shape parameter” $\Gamma \sim \Omega h$: we find 297.3 clusters for $h = 0.64$. Finally, assuming a fixed f_{ICM} , the mass corresponding to a constant SZ decrement scales more strongly, as $M_{\min} \propto h^{-8/5}$ (with the f_{ICM} dependence used in this paper, the dependence would be weaker). Under this scaling, including the h -dependence of the power spectrum, we find 291.5 clusters for $h = 0.64$, implying that based on the number counts alone, models with $h = 0.64$ and $h = 0.65$ would only be 0.5σ apart. We conclude that in the case of constraints on h , we can directly compare the likelihood and the 2D-KS test performances, both of which will test primarily the shapes, rather than the normalizations, of the underlying distributions.

The observation of a discrete number N clusters is a Poisson process, the probability of which is given by the product

$$P = \prod_{i=1}^N (e_i^{n_i} \exp[-e_i]/n_i!) \quad (15)$$

where n_i is the number of clusters observed in the i^{th} experimental bin, and e_i is the expected number in that bin in a given model: $e_i = I(\vec{x}_i)\delta\vec{x}_i$. Here, I is proportional to the probability distribution, and \vec{x} denotes the set of observables, in the present case, $\vec{x} = (\eta, z_o)$. Following Cash (1979), for unbinned data (or equivalently for very small bins that have only 0 or 1 counts) we define the quantity

$$C \equiv -2 \ln P = 2(E - \sum_{i=1}^N \ln I_i), \quad (16)$$

where $N = 300$ is the total number of observed clusters (i.e. the number of clusters in the mock catalog for our fiducial model with $h = 0.65$), E is the expected number of clusters in models with arbitrary h . We have omitted all terms that involve $\delta\vec{x}_i$ since they do not depend on h . The quantity ΔC , defined in two models with different h , has a χ^2 distribution (e.g. Cash 1979). Both the 2D-KS test and the maximum likelihood test are performed in the

$\eta - z_o$ plane, where $I(\eta, z_o)$ is given by:

$$I(\eta, z_o) \equiv \frac{d^2 N}{d\eta dz_o} \quad (17)$$

where

$$\begin{aligned} \frac{d^2 N}{d\eta dz_o} &= \frac{dn}{d\eta} \frac{dV}{dz_o d\Omega} \Delta\Omega \\ &= \left(\frac{d\eta}{dz_f} \right)^{-1} \int_{M_{\min}}^{\infty} \frac{dN}{dM} \Big|_{z_o} dM \frac{dP}{dz_f} \frac{dV}{dz_o d\Omega} \Delta\Omega. \end{aligned} \quad (18)$$

Here dN/dM is the Press–Schechter mass function, dP/dz is the formation redshift distribution from Lacey & Cole (1993), and $dV/dz d\Omega$ is the comoving cosmological volume. We have assumed a solid angle $\Delta\Omega = 20 \text{ deg}^2$, and included clusters at redshifts $0.1 < z < 1$ in our analysis. Recall also that

$$\eta = h \frac{(1+z_f)^3 \varphi(z_f)}{(1+z_o)^3 \varphi(z_o)}. \quad (19)$$

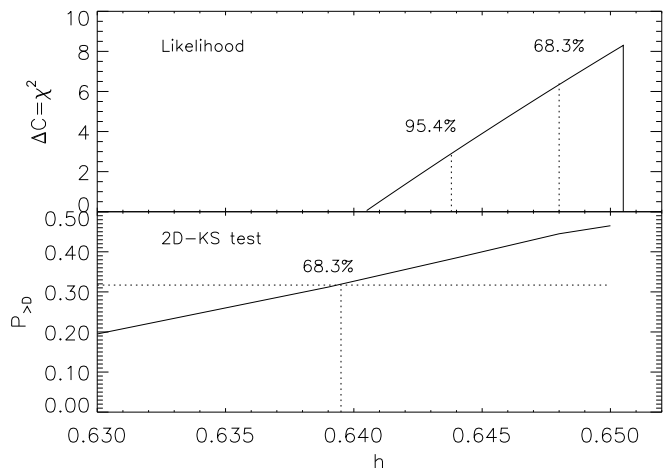


Fig. 13.— Comparison of 2D-KS and maximum likelihood confidence levels. Since the cluster abundance is insensitive to h it is possible to directly compare the performances of the two tests for a sample of 300 clusters in our fiducial (deterministic) model. The likelihood is obtained following equations (16) and (19). The maximum likelihood method is much more sensitive than the KS test, but it requires good knowledge of the cluster mass function and of mask and selection effects of the survey.

In Figure 13, we show the comparison between the likelihoods obtained from ΔC and the from the 2D-KS confidence levels, as a function of h . Since the likelihood is non-Gaussian, the confidence levels have been obtained by integrating the likelihood curve. The figure reveals that the likelihood method is more sensitive than the KS test. For example, in the KS case, the model with $h = 0.64$ is approximately 1σ away from the fiducial $h = 0.65$ model, while the ΔC test puts this model at $> 2\sigma$ significance. This finding suggests that a maximum likelihood method better captures the shape of the η vs z distribution of clusters, and can significantly improve on the statistical constraints quoted here. We expect that a similarly improved

use of the distribution shapes may be possible in other cases (e.g., in the measurements of Ω_0). However, constraints obtained from a likelihood analysis can be dominated by the information available from the total cluster abundance, rather than the shape. In those cases, and improved utilization of the shapes can result in only marginal improvements of the overall constraints, and, at the same time, the use of the maximum likelihood method would subject the results to additional systematic errors. A systematic study of the best statistic in each case is beyond the scope of the present paper, and is deferred to a future publication.

8. DISCUSSION

In anticipation of extensive data on a large sample of galaxy clusters, it is important to analyze cluster properties to reduce systematic errors; to test whether physical properties of the local cluster sample are preserved at high redshift and, if necessary, to model their evolution. We present a first attempt to do so self-consistently from cluster data.

The approach presented here assumes that the primordial fluctuation field was Gaussian. However, clusters are rare peaks of the density fluctuation and are therefore extremely sensitive to small deviations from gaussianity. Nevertheless, this assumption is not crucial: a parameterization of non-gaussianity could easily be included in the model (e.g., Robinsor, Gawiser & Silk 1999; Matarrese, Verde & Jimenez 2000; Verde et al. 2000; Verde et al. 2001).

We have used four observables: the redshift, the X-ray temperature, the total observed SZ flux decrement, and the cluster angular size. A particular worry in our approach is that we estimate the angular size based on the virial radius. Current numerical simulations of cluster formation (see, e.g., Bryan & Norman 1998) indeed indicate the presence of a virialization shock, as expected from the top-hat collapse model. However, the shock tends to be weaker, and located at larger radii, which can make its detection in the SZE maps difficult, or impossible. Cluster angular sizes can also be estimated from X-ray maps, which, however, effectively probe only the core radius.

Alternatively, similar scaling relations could be obtained by considering other observables, in addition to those we have considered here. The “fundamental plane” approach can be generalized to include, for example, the X-ray luminosity, the velocity dispersion, or estimates of the cluster masses (e.g. from weak lensing). This opens up many interesting possibilities. The constraints on clusters physics and cosmological parameters are complementary to constraints obtained from other observables; they could thus be combined together not only with e.g., CMB constraints but also with constraints obtained e.g., from X-ray clusters abundances, SZE cluster abundances, analysis of kinetic SZE and weak lensing statistics.

9. CONCLUSIONS

In view of the advent of high-precision cosmology and the expected avalanche of cluster data available with SZ experiments in conjunction with X-ray missions, it is vital

to be able to extract the maximum amount of information from these cluster samples.

We have investigated the scientific potential of obtaining total observed SZ flux decrements (ΔS_ν) in the context of a well studied cluster sample, for which X-rays and optical follow-up are available. In particular, for cosmological studies, one would ideally like to use clusters as “standard candles”: the use of large future galaxy cluster surveys for cosmological studies is likely to be limited by the validity of this assumptions, rather than by statistical uncertainties (Haiman, Mohr & Holder 2001).

We used a semi-analytic model to study the expected distribution of galaxy clusters in redshift (z), virial temperature (T), Sunyaev–Zeldovich decrement (ΔS_ν), and angular size (θ). In the simplest models, clusters are identified with virialized, spherical halos. In this case, at every redshift, clusters define a “fundamental plane” (FP) in the three dimensional parameter space ($T, \Delta S_\nu, \theta$). The FP and its redshift–evolution are sensitive to both the internal evolution of clusters, and to the underlying cosmological parameters, and can be used to obtain useful constraints on both. We have parameterized possible deviations from this model to include effects of energy injection or feedback, stochastic scatter in the observables ($T, \Delta S_\nu, \theta$), and deviations from virial equilibrium. We have shown that their effect is to create measurable deformations in the FP.

We have thus derived predictions for clusters scaling relations that involve the SZ decrement, and studied how these scaling relations depend on assumptions about the cluster physics and structure (i.e. on the assumption that

clusters are standard candles), as well as on the underlying cosmological parameters. In particular, we find that, if clusters are virialized objects, the cluster distribution in the $\Delta S_\nu - T$ plane should be narrow. The predicted tightness of the $\Delta S_\nu - T$ relation makes it especially useful for quantifying clusters physical properties, possible deviations from virialization, and to detect the presence of stochastic scatter in $(T, \Delta S_\nu, \theta)$, i.e. it is a useful tool to test whether clusters can be used as “standard candles”.

On the other hand, under the assumption that clusters can be used as “standard candles”, we show that deformations of the fundamental plane and of clusters scaling relations that involve ΔS_ν , can be used to determine cosmological parameters. The constraints on cosmological parameters so obtained are complementary to those obtained e.g., from CMB primary anisotropies, cluster abundances, or clusters central SZ decrements.

Our results show that the choice of statistic can have a significant impact on the derived constraints, at the level of a factor of several on the constrained parameters.

ACKNOWLEDGMENTS

We thank Joe Mohr and G. Holder for many stimulating discussions, and G. Bryan, U. Seljak & J. P. Hughes for useful comments. LV acknowledges NASA grant NAG5-7154 and thanks Caltech, where part of this research was completed, for hospitality. ZH is supported by NASA through the Hubble Fellowship grant HF-01119.01-99A, awarded by the Space Telescope Science Institute, which is operated by the Association of Universities for Research in Astronomy, Inc., for NASA under contract NAS 5-26555.

REFERENCES

- Bahcall, N. A., & Cen, R. Y. 1992, ApJ, 398, L81
 Bahcall, N. A., & Cen, R. Y. 1993, ApJ, 407, L49
 Bahcall, N. A., & Fan, X. 1998, ApJ, 504, L1
 Bennett, C. L. et al. 1995, BAAS, 187.7109; see also <http://MAP.gsfc.nasa.gov>
 Bersanelli et al 1996, COBRAS/SAMBA Rep. Phase A study, ESA D/SCI(96)3; see also <http://astro.estec.esa.nl/PLANCK/>
 Bialek, J. J., Evrard, A. E., & Mohr, J. J. 2001, ApJ, submitted, astro-ph/0010584
 Birkinshaw, M. 1979, MNRAS, 187, 847
 Birkinshaw, M. 1998, Phys. Rep., 310, 97
 Blanchard, A. & Bartlett, J.G. 1998, A&A, 332, L49
 Bryan, G. L. 2001, ApJ, in press, astro-ph/0009286
 Bryan, G. L. & Norman, M. L. 1998, ApJ, 495, 80
 Burles, S., & Tytler, D. 1998, ApJ, 499, 699
 Mauskopf, et al. 1999, astro-ph/9911444
 de Bernardis, et al. 2000, Nature 404, 955
 Carlstrom, J. E. et al. 2000, in New Cosmological Data and the Values of the Fundamental Parameters, International Astronomical Union. Symposium no. 201, 48
 Cash, W. 1979, ApJ, 228, 939
 Eke, V. R., Cole, S., & Frenk, C. S. 1996, MNRAS, 282, 263
 Eke, V. R., Navarro, J. F., & Frenk, C. S. 1998, ApJ503, 569
 Evrard, A. E. 1989, ApJ, 341, L71
 Evrard, A. E. 1990, ApJ, 363, 349
 Evrard, A. E., Henry J. P. 1991, ApJ, 383, 95
 Evrard, A. E., Metzler, C., & Navarro, J. F. 1996, ApJS, 469, 494
 Fasano, G. & Franceschini A. 1987, MNRAS, 225, 155
 Finoguenov, A., Reiprich, T. H., & Böhringer, H. 2000, astro-ph/0010190
 Grego, L. et al. 2000, astro-ph/0012067
 Grego, L. et al. 2000, ApJ, 539, 39
 Gunn, J. E. 1978, in Observational Cosmology, ed. Maeder, A., Martinet, L., & Tammann, G., Geneva Observatory.
 Haiman, Z., Mohr, J. J., and Holder, G. P. 2001, ApJ, in press, astro-ph/0002336
 Henry, J. P., & Arnaud, K. A. 1991, ApJ, 372, 410
 Holder, G.P., Mohr, J.J., Carlstrom, J.E., Evrard, A.E. & Leitch, E.M. 2000, ApJ, in press, astro-ph/9912364
 Holder, G.P., Haiman, Z. & Mohr, J.J., astro-ph/0105396
 Horner, D. J., Mushotzky, R. F., & Scharf, C. A. 1998, ApJ, 520, 78
 Jaffe, A., et al. 2000, Phys. Rev. Lett., in press, astro-ph/0007333
 Jenkins, A. et al. 2000, MNRAS, submitted, astro-ph/0005260
 Jones, M. E. et al. 2001, MNRAS in press, astro-ph/0103046
 Joy M., et al. 2001, ApJLett, 551, 1
 Kaiser, N. 1991, ApJ, 383, 104
 Kay, S. T., Liddle, A. R., & Thomas, P. A. 2001, MNRAS, astro-ph/0102352
 Kitayama, T., & Suto, Y. 1996, ApJ, 469, 480 [KS96]
 Kneissl R. et al. 2001, MNRAS in press, astro-ph/0103042
 Lacey, C., & Cole, S. 1993, MNRAS, 262, 627 [LC93]
 Lilje, P. B. 1992, ApJ, 386, L33
 Mandolesi et al. 1998, proposal submitted to ESA for the Planck low frequency instrument
 Matarrese, S., Verde, L., & Jimenez, R. 2000, ApJ, 541, 10
 Mason, B. S., Myers S. T., Readhead, A. C. S. 2001, astro-ph/0101169
 Myers, S. T., Baker J. E., Readhead, A. C. S., Leitch, E. M., Herbig, T. 1997, ApJ, 485, 1
 Mathiesen, B. F. 2000, astro-ph/0012117
 McDonald, P., Miralda-Escude, J. 1999, ApJ, 518, 24
 Mohr, J. J., Reese, E. D., Ellingson, E., Lewis, A. D., & Evrard, A. E. 2000, ApJ, in press, astro-ph/004242
 Mohr, J. J., & Evrard, A. E., 1997, ApJ, 491, 38
 Mohr, J. J., Mathiesen, B., & Evrard, A. E., 1999, ApJ, 517, 627
 Muanwong, O., Thomas, P. A., Kay, S. T., Pearce, F. R., & Couchman, H. M. P. 2001, astro-ph/0102048
 Navarro, J. F., Frenk, C. S. & White, S. D. M. 1995, MNRAS, 275, 720
 Oukbir, J., & Blanchard, A. 1992, A&A, 262, L21
 Page, L., et al. 2001, in preparation
 Peacock, J. A. 1993, MNRAS, 202, 615
 Peebles, P. J. E. 1980, Large-Scale Structure of the Universe, Princeton Univ. Press
 Perlmutter, S. et al. 1998, ApJ, 517, 565
 Pierpaoli, E., Scott, D., & White, M. 2000, MNRAS, in press, astro-ph/0010039
 Press, W.H., Teukolsky, S.A., Vetterling, W.T., & Flannery, B.P.

- 1992, Numerical Recipes in Fortran, 2nd ed., Cambridge University Press, Cambridge, UK
- Press, W. H., & Schechter, P. L. 1974, ApJ, 181, 425
- Reese, E. D. et al. 2000, ApJ, 533, 38
- Reiss A. G. et al. 1998, ApJ, 507, 46
- Robinson, J., Gawiser, E., & Silk, J. 1999, ApJ, astro-ph/9906156
- Roettiger, J., Loken, K., & Burns, J. 1997, ApJS, 109, 307
- Roukema B., F., Mamon G. A., “The large-scale structure peak as a comoving standard ruler”, IAU symposium, 2000, 201, E38
- Sasaki, S. 1994, PASJ, 46, 427
- Sheth, R., Mo, H. J., & Tormen, G. 1999, astro-ph/9907024
- Silk, J., White, S. D. M., ApJ, 226, L103
- Sugiyama, N. 1995, ApJSuppl., 100, 281
- Sunyaev, R. A., & Zeldovich, Ya. B. 1980, ARA&A, 18, 537
- Tucker, W., Blanco, P., Rappaport, S., David, L., Fabricant, D., Falco, E. E., Forman, W., Dressler, A., & Ramella, M. 1998, ApJ, 496, L5
- Verde, L., Jimenez, R., Kamionkowski, M., & Matarrese, S. 2001, MNRAS
- Verde, L., Kamionkowski, M., Mohr, J. J., Benson, A. J., 2000, MNRAS, in press, astro-ph/0007426
- Viana, P. T. P., & Liddle, A. R. 1996, MNRAS, 281, 323
- Viana, P. T. P., & Liddle, A. R. 1999, MNRAS, 303, 535
- Wang, L., & Steinhardt, P. J. 1998, ApJ, 508, 483
- White, S. D. M., Efstathiou, G., & Frenk, C. S. 1993, MNRAS, 262, 1023
- Willick, J., A. 2000, ApJ, 530, 80
- Xu, H., Jin, G., & Wu, X. 2001, astro-ph/0101564